water

MDPI

Article

Unraveling the Complexities of Groundwater Salinization in Coastal Environments: Insights from Laizhou Bay's Eastern Coast, China

Peng Huang, Chuanming Ma * and Aiguo Zhou

School of Environmental Studies, China University of Geosciences, Wuhan 430000, China; hpses@cug.edu.cn (P.H.); aiguozhou@cug.edu.cn (A.Z.)
* Correspondence: machuanming@cug.edu.cn; Tel.: +86-027-67883159

Abstract: Coastal areas have made substantial contributions to global economic development but are plagued by challenges such as groundwater salinization. Groundwater serves as the primary source for drinking, industrial, and domestic purposes in these coastal areas. Therefore, understanding the causes and processes of groundwater salinization holds paramount significance for effective groundwater management. The coastal area of Laizhou Bay in northern China serves as a quintessential example of such a scenario. With substantial groundwater extraction and severe groundwater salinization issues, it exacerbates the disparity between water-resource supply and demand. Currently, our understanding of the processes and influencing factors related to groundwater salinization in this region remains limited. In this study, employing hydrochemical and stable chlorine isotope analyses on 35 groundwater and seawater samples, an in-depth investigation into the complex mechanisms underlying groundwater salinization in the Quaternary aquifers of the eastern coastal plain of Laizhou Bay was conducted. The test results of the samples indicate that brine and saline groundwater are primarily of the Na-Cl type, exhibiting a hydrochemical composition similar to that of seawater. Brackish groundwater exhibits a diverse hydrochemical composition. The hydrogen and oxygen isotope characteristics of brackish and fresh groundwater resemble atmospheric precipitation, while brine, seawater, and saline groundwater show hydrogen and oxygen isotope depletion. Compared to seawater, brine exhibits significant $\delta^{37}Cl$ depletion. The analysis of the test results reveals that the formation of brine aquifers results from a complex interplay of climate change, tectonic movements, and sea–land evolution, involving lagoon development during seawater regression, salt concentration through evaporation, and subsequent water–rock interactions. The genesis of saline groundwater involves a complex interplay of brine–seawater mixing, significant evaporation, and potential input of fresh groundwater from atmospheric precipitation and river sources. The formation of brackish groundwater is predominantly influenced by atmospheric precipitation, and agricultural activities, with significant variations in NO_3^- concentrations attributed to varying intensities of fertilizer application in the northern plain area. These insights contribute to a deeper understanding of the origins of groundwater and can inform the development of policies for groundwater protection in this area.

Keywords: hydrochemistry; hydrogen and oxygen isotope; chlorine isotope; groundwater salinization; Laizhou Bay

Citation: Huang, P.; Ma, C.; Zhou, A. Unraveling the Complexities of Groundwater Salinization in Coastal Environments: Insights from Laizhou Bay's Eastern Coast, China. *Water* **2023**, *15*, 3629. https://doi.org/10.3390/w15203629

Academic Editor: Adriana Bruggeman

Received: 4 September 2023
Revised: 14 October 2023
Accepted: 15 October 2023
Published: 17 October 2023

1. Introduction

Roughly three-quarters of the world's nations are coastal states [1]. Currently, approximately 17% of the global population resides in coastal regions [2]. Coastal areas are marked by high population density, economic prosperity, and delicate ecological ecosystems, frequently grappling with environmental challenges, such as the salinization of groundwater [3,4]. Groundwater serves as a primary source of drinking water and sustenance for production and livelihoods in coastal regions [5]. The identification of the

causes of groundwater salinization in coastal aquifers is of paramount significance for the scientific management and utilization of groundwater resources in these regions.

Numerous factors contribute to the salinization of groundwater. In its natural state, a hydraulic connection exists between seawater and coastal aquifers. Seawater infiltrates these coastal aquifers in a wedge-like fashion due to disparities in hydraulic pressure and density between seawater and groundwater. This dynamic equilibrium is upheld, usually. However, excessive groundwater extraction results in an ongoing decline in groundwater levels, disrupting this equilibrium and causing seawater to encroach inland, resulting in seawater intrusion [6–10]. On the other hand, groundwater salinization may also be influenced by factors such as groundwater evaporation [11], groundwater mixing [12,13], water–rock interactions [14], and human-induced pollution [15,16]. Furthermore, climate change can lead to fluctuations in sea levels, altering the conditions for groundwater recharge in coastal areas, thereby adversely affecting groundwater resources and the environment [17–20].

As early as the 1960s, concerns regarding seawater intrusion had arisen in China's coastal aquifers, with particularly severe challenges evident along the coastline of Laizhou Bay [21]. This issue intensified, expanding inland at a rate of 12% per year [7,21]. Previous investigations into groundwater salinization along the Laizhou Bay coast have primarily centered on the southern shoreline [22–24]. The eastern shores of Laizhou Bay are characterized by a predominant presence of agricultural, mining, aquaculture, and salt-farming industries, resulting in diverse land-use patterns, including the establishment of an artificial island. The annual groundwater extraction in this region amounts to 1.54×10^8 m^3, further exacerbating the existing disparities in water supply and demand [25]. Research efforts directed towards the eastern shores of Laizhou Bay have predominantly revolved around groundwater quality assessment and groundwater management [26,27]. Our understanding of the processes and influencing factors contributing to groundwater salinization in this specific area remains limited [25].

By analyzing hydrochemical and isotopic data in conjunction with geological and hydrogeological conditions, an assessment of groundwater salinization can be undertaken [28]. The utilization of a Piper diagram facilitates the categorization of groundwater types and the interpretation of groundwater chemistry [29–32]. Hydrochemical facies evolution diagrams and Gibbs diagrams serve as valuable tools for elucidating the processes and mechanisms involved in groundwater evolution [33–38]. Traditional hydrochemical methods regard Cl^- and Br^- as conservative tracers for interpreting the origin of groundwater due to their non-involvement in other mineral-formation processes. Specific ion ratios, such as Cl/Br, can be employed to explore the origin and evolution of groundwater [39–42]. When Cl and Br stem from the same source, the Cl/Br ratio should remain constant [43]. However, in the presence of alternative pathways for Cl and Br input, or when processes involving convective-diffusion mixing of saline solutions occur, the applicability of the Cl/Br ratio may diminish [44]. Statistical methodologies, coupled with geological and hydrogeological conditions, have been applied in groundwater salinization investigations [45–48], as have mathematical models [49–54]. These approaches enhance our comprehension of groundwater salinization processes and contribute to effective management strategies.

H and O are fundamental constituents of water molecules, and hold paramount importance in hydrogeochemical processes. H exists in two stable isotopic forms, ^1H and ^2H, with a relative abundance ratio of ^1H:^2H = 99.9844:0.01557 [55]. O exhibits three stable isotopes, ^{16}O, ^{17}O, and ^{18}O, with relative abundances in the atmosphere of ^{16}O:^{17}O:^{18}O = 99.759:0.2039:0.0374 and in seawater of ^{16}O:^{17}O:^{18}O = 99.762:0.200:0.038 [55]. During the process of water evaporation, H and O undergo fractionation, with the heavier isotopes preferentially accumulating in the remaining water [56]. Due to common disparities in H and O isotope composition among water sources, the stable isotope ratios of ^2H and ^{18}O in water remain unaffected by geochemical processes within the aquifer [57,58]. Consequently, they find an application in groundwater-salinization research, serving as a foundation for comprehending the origins and mixing mechanisms of groundwater [59–63].

Chloride (Cl) stands as a conservative hydrophilic element, demonstrating mobility across the lithosphere, hydrosphere, and atmosphere. Cl has two stable isotopes, with a ratio of ^{37}Cl:^{35}Cl = 0.32 [1]. Cl plays a vital role in diverse Earth processes, spanning the Earth's crust, cycling within oceanic crusts [64], geothermal phenomena [65], interactions between water and rocks [66], origins of fluid salinity [67], historical deposition of marine crustal fluids [68], and fluid cycling during subduction processes [69,70]. In seawater, Cl^- exhibits exceedingly high concentrations, and it undergoes substantial isotope fractionation during the formation and evolution of brine. Utilizing Cl isotopes proves highly effective in characterizing the evolution of groundwater in coastal regions, particularly in locales with elevated chloride concentrations [71]. Owing to the presence of diffusion processes, a notable isotopic fractionation of approximately 2.1‰ occurs in shallow groundwater, with the migration rate of ^{35}Cl surpassing that of ^{37}Cl [72,73].

To gain a deeper understanding of the processes and mechanisms involved in groundwater salinization in the eastern coast of Laizhou Bay, and to provide scientific insights for the management of seawater intrusion and dynamic groundwater quality control, this study employed an integrated method combining hydrochemical analysis, stable H-O isotopes, and stable Cl isotopes to investigate the crucial hydrochemical processes influencing groundwater in the eastern coastal plain of Laizhou Bay, and analyzed the processes and mechanisms of groundwater salinization. The findings of this study can provide vital insights for effectively preventing and managing seawater intrusion and ensuring the sustainable utilization of groundwater resources.

2. Materials and Methods

2.1. Study Area

The study area is located in the northern region of Shandong Province, China, along the eastern coastline of Laizhou Bay (Figure 1). It experiences an average annual temperature of 12 °C, and receives an average annual precipitation of 610 mm. The topography in the study area slopes from southeast to northwest, with the highest elevation point reaching 623.56 m above sea level and the lowest point at 0.32 m. The study area is characterized by predominantly small to medium-sized rivers, with many originating in the mountainous areas to the southeast.

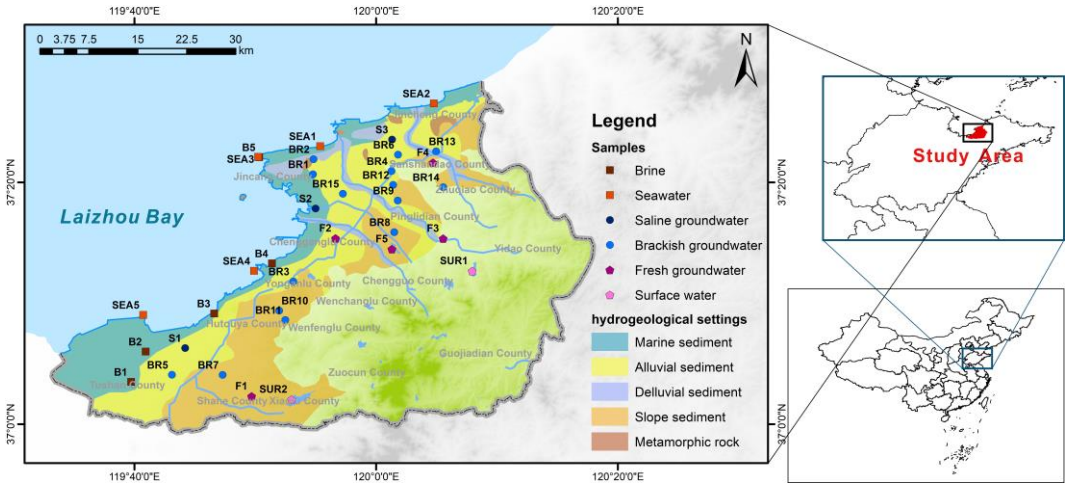

Figure 1. Hydrogeological conditions and samples in the study area.

The sedimentary facies of the aquifer change from southeast to northwest, transitioning from alluvial deposits to fluvial deposits, and finally to marine sediments in the coastal plains. Groundwater in this study area primarily comprises unconsolidated rock porous water and fractured bedrock water. In the coastal plain aquifers, fine sand and silt dominate, with thicknesses ranging from 3 to 10 m. Typically, groundwater levels remain within 4 m of the surface, and the water is often brackish or saline. In piedmont alluvial plains, the

aquifers consist mainly of fine sand, medium-coarse sand, and gravel, with thicknesses spanning from 2 to 10 m. Groundwater levels in this region also typically lie within 4 m of the surface. Fractured bedrock aquifers are primarily located in the eastern and southern parts of the study area, with fractures being less developed. The mountainous areas and the unconfined portions of the aquifer constitute the primary recharge zones, and the typical natural groundwater flow pattern is from southeast to northwest, although this general flow pattern may be altered due to high-permeability incised channels crossing the area [7].

The mineralogy of the shallow aquifer includes quartz, plagioclase feldspar, sodium feldspar, orthoclase feldspar, muscovite, biotite, kaolinite, calcite, dolomite, illite, smectite, and calcium-montmorillonite. In some areas, there are limited occurrences of evaporites such as gypsum, anhydrite, halite, polyhalite, mirabilite, and trona [7]. In the southeastern mountainous region, the bedrock primarily consists of Cretaceous and Neogene basalts, andesites, sandstones, and volcanic clastic rocks, comprising plagioclase, sodium feldspar, potassium feldspar, and biotite [7].

2.2. Samples and Hydrochemistry Analyses

The sampling took place in September 2020 along the eastern shores of Laizhou Bay, as depicted in Figure 1. A total of 35 samples were collected, comprising 28 groundwater samples, 5 seawater samples, and 2 surface water samples. On-site measurements included pH and electrical conductivity, while alkalinity was determined through acid-base titration within a 24 h window. For hydrochemistry and H-O isotope analysis, samples were initially filtered on-site using 0.45 μm filter heads. Subsequently, they were transferred into three 50 mL polyethylene bottles, with one of these bottles having nitric acid added to achieve a pH < 2 for cation analysis. Samples intended for Cl isotope analysis were carefully placed in 1000 mL polyethylene bottles, filled, and purged of any air bubbles.

The analysis of major and trace elements was conducted at the Analysis and Testing Center, School of Environmental Studies, China University of Geosciences. Cation analysis was performed using an Inductively Coupled Plasma-Atomic Emission Spectrometer (ICP-AES), while anion analysis was conducted using Ion Chromatography (IC). The analytical error was below ±5% [74].

The ion balance error (IBE) was utilized to assess the reliability of hydrochemical data, which was calculated with the following Equation (1).

$$IBE = \frac{R_{cation} - R_{anion}}{R_{cation} + R_{anion}} \times 100\% \quad (1)$$

In Equation (1), R_{cation} represents cation concentration expressed in milliequivalents per liter (meq/L), while R_{anion} represents anion concentration. Following examination, all hydrochemical data has been confirmed as reliable.

Following the standards set by Fetter (2018) [75] and Salas et al. (2014) [76], groundwater samples were categorized based on their total dissolved solids (TDS) into four distinct groups: brine samples (TDS > 100 g/L, 5 samples), saline groundwater samples (10 g/L < TDS < 100 g/L, 3 samples), brackish groundwater samples (1 g/L < TDS < 10 g/L, 15 samples), and fresh groundwater samples (TDS < 1 g/L, 5 samples).

2.3. Stable Isotope Analyses

H and O isotopes were analyzed at the State Key Laboratory of Biogeology and Environmental Geology, China University of Geosciences, using a Thermal Conversion/Elementary Analyzer (TC/EA) coupled with Isotope Ratio Mass Spectrometry (IRMS). The test results were normalized to Vienna Standard Mean Ocean Water (V-SMOW), with testing errors for δ^2H and $\delta^{18}O$ being ±1.0‰ and ±0.1‰, respectively [77].

Stable Cl isotopes were analyzed at the Salt Lake Chemistry Analysis and Test Center, Qinghai Institute of Salt Lakes, Chinese Academy of Sciences, utilizing Isotope Ratio Mass Spectrometry (IRMS) in conjunction with a Gas Bench-II device. Before analysis, all Cl was

converted into CH_3Cl. The resulting data were normalized using the Standard Mean Ocean Chlorine (SMOC) standard, and the testing error was determined to be ±0.08‰ [78].

3. Results

3.1. Hydrochemistry Compositions

The hydrochemistry data for the samples are provided in Table S1. A distinct pattern in groundwater salinity and hydrochemical composition emerges from southwest to northeast. As it transitions from the mountainous regions to the plains, there is a gradual increase in total dissolved solids (TDS) in the water, ranging from 0.70 g/L to 832.91 g/L. Employing the Shoka Lev classification method [79] to classify the water samples, both brine and saline groundwater predominantly exhibit a Na-Cl hydrochemical type. Notably, sample B1 stands out with a Na·Mg-Cl classification. Brackish groundwater displays regional variations, with the northern sector predominantly characterized by a Na·Ca-Cl·HCO_3 type, while the southern region exhibits a more diverse range of hydrochemical types. These variations are significantly influenced by local geological conditions and human activities. Fresh groundwater samples are primarily classified into Na·Ca-HCO_3·Cl, Na·Ca-Cl·HCO_3, and Ca·Na-HCO_3·Cl hydrochemical types. Seawater showcases a Na-Cl hydrochemical type, while sample SUR1 falls into the Na-Cl·SO_4 category, and sample SUR2 is classified as Na·Ca-Cl·HCO_3.

The hydrochemical compositions of groundwater, seawater, and surface water in the study area are depicted in Figure 2. The hydrochemical compositions of brine and saline groundwater bear a resemblance to seawater, indicating their common marine origin. In contrast, the hydrochemical composition of brackish groundwater significantly differs from that of seawater, suggesting that brackish groundwater has an origin unrelated to seawater.

The hydrochemical control mechanisms of natural water bodies are classified into three categories in the Gibbs diagram, namely precipitation-dominated, rock weathering-dominated, and evaporation-concentration-dominated [80]. As depicted in Figure 3, it is evident that the hydrochemical control mechanisms vary significantly among different samples. Brine and saline groundwater samples are situated in the upper-right quadrant of the Gibbs diagram, positioned above the seawater samples, signifying their pronounced control by intense evaporation and concentration processes. Conversely, brackish groundwater and fresh groundwater are located in the lower-right quadrant of the Gibbs diagram, indicating that their formation is predominantly governed by precipitation.

Cl and Br are soluble halogens with similar properties in seawater and constant-concentration fresh groundwater [81]. At low temperatures, both Cl and Br exhibit minimal involvement in ion exchange processes and mineral adsorption. Cl/Br ratios are typically used to analyze groundwater salinization in cases where TDS exceeds 2–3 g/L [82]. In this study, Cl/Br serves as an indicator to identify the sources of salinity in brine and saline groundwater. The Cl/Br ratio in Bohai Sea water ranges from 650 to 657, closely approximating that of standard seawater (Cl/Br = 655, Cl = 550 mmol/L, Br = 0.84 mmol/L) [83]. However, the Cl/Br ratios in this study are slightly lower than those in Bohai Sea water and standard seawater (Figure 4a), possibly due to the proximity of the sampling points to the coast, which may have been influenced by groundwater inputs. The resemblance of Cl/Br ratios in brine and saline groundwater to seawater indicates that their salinity originates from seawater [84]. The Cl/Br ratios in these samples do not fall within the range of 1200 to 6600, signifying a negligible impact from evaporative dissolution processes in these brine and saline groundwater samples [85].

Figure 4 depicts the relationships among Ca^{2+}, Na^+, K^+, Mg^{2+}, Si^{4+}, $SO_4{}^{2-}$, $HCO_3{}^-$, and Br^-, with ion concentrations normalized relative to the Br^- concentration. As the Br^- concentration increases, brine and saline groundwater exhibit only minor fluctuations in the ratios of cation concentrations to Br^- concentration, providing evidence of their marine origin for salinity.

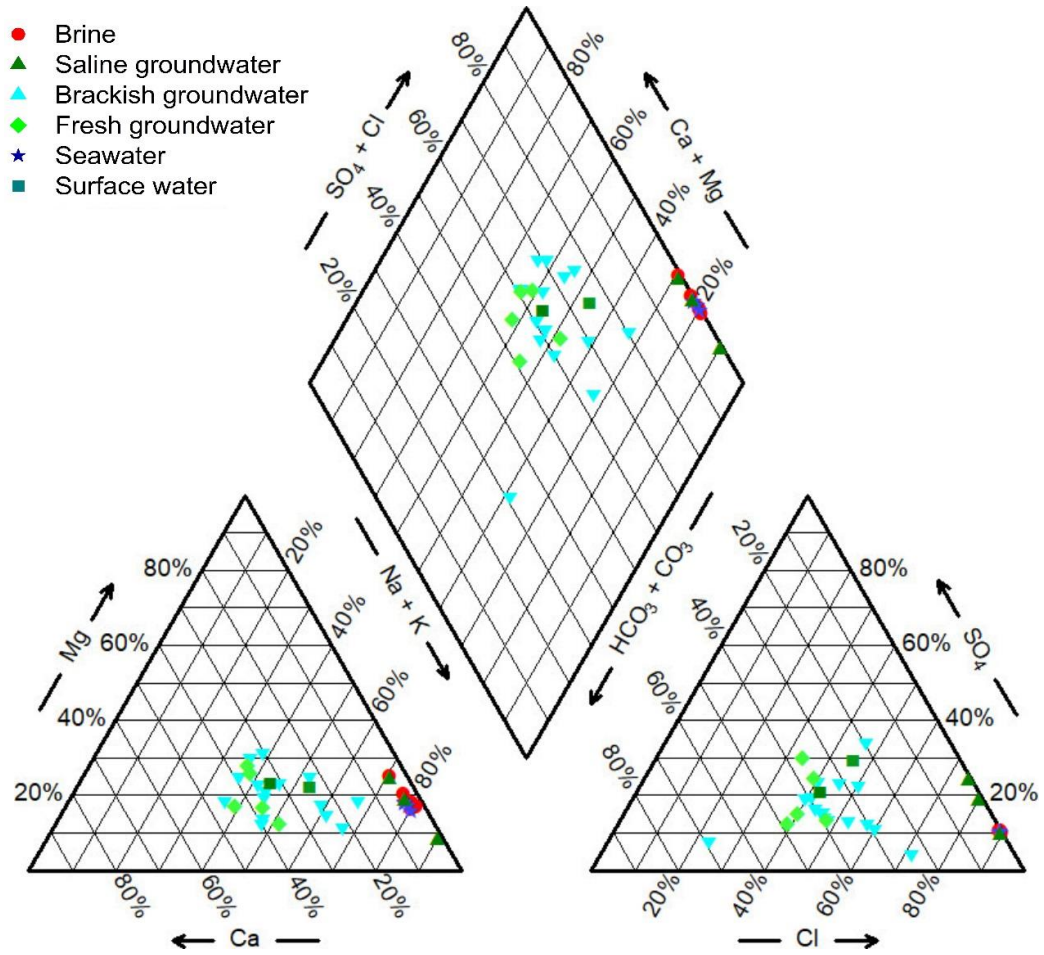

Figure 2. Piper diagram of all water samples.

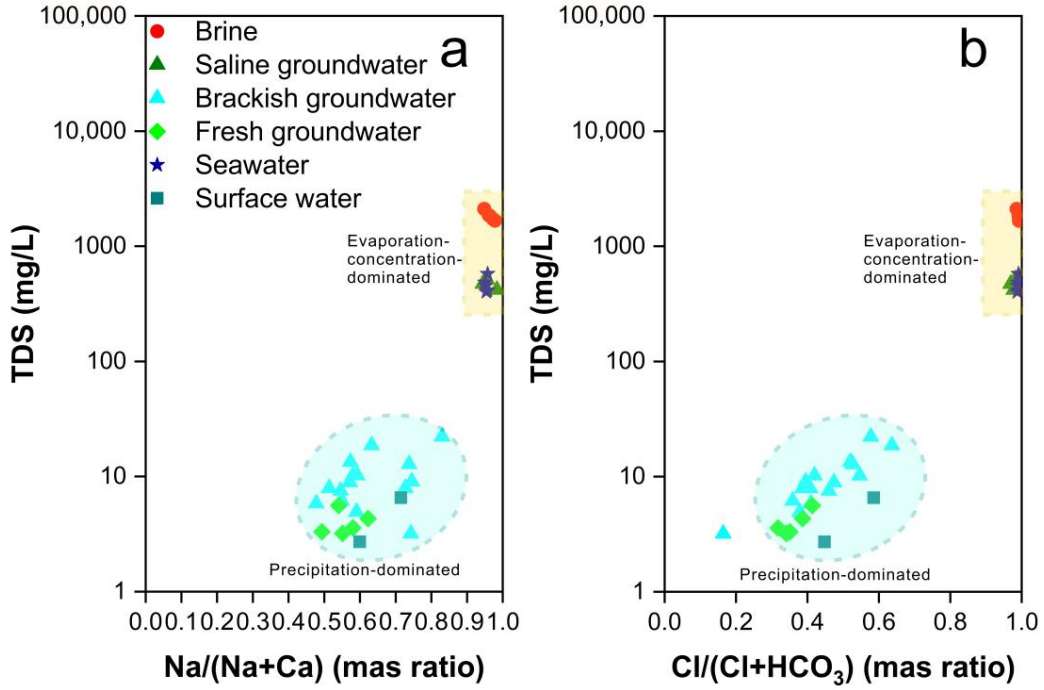

Figure 3. Gibbs diagrams of all water samples. (**a**) Cation Gibbs diagram (**b**) Anion Gibbs diagram.

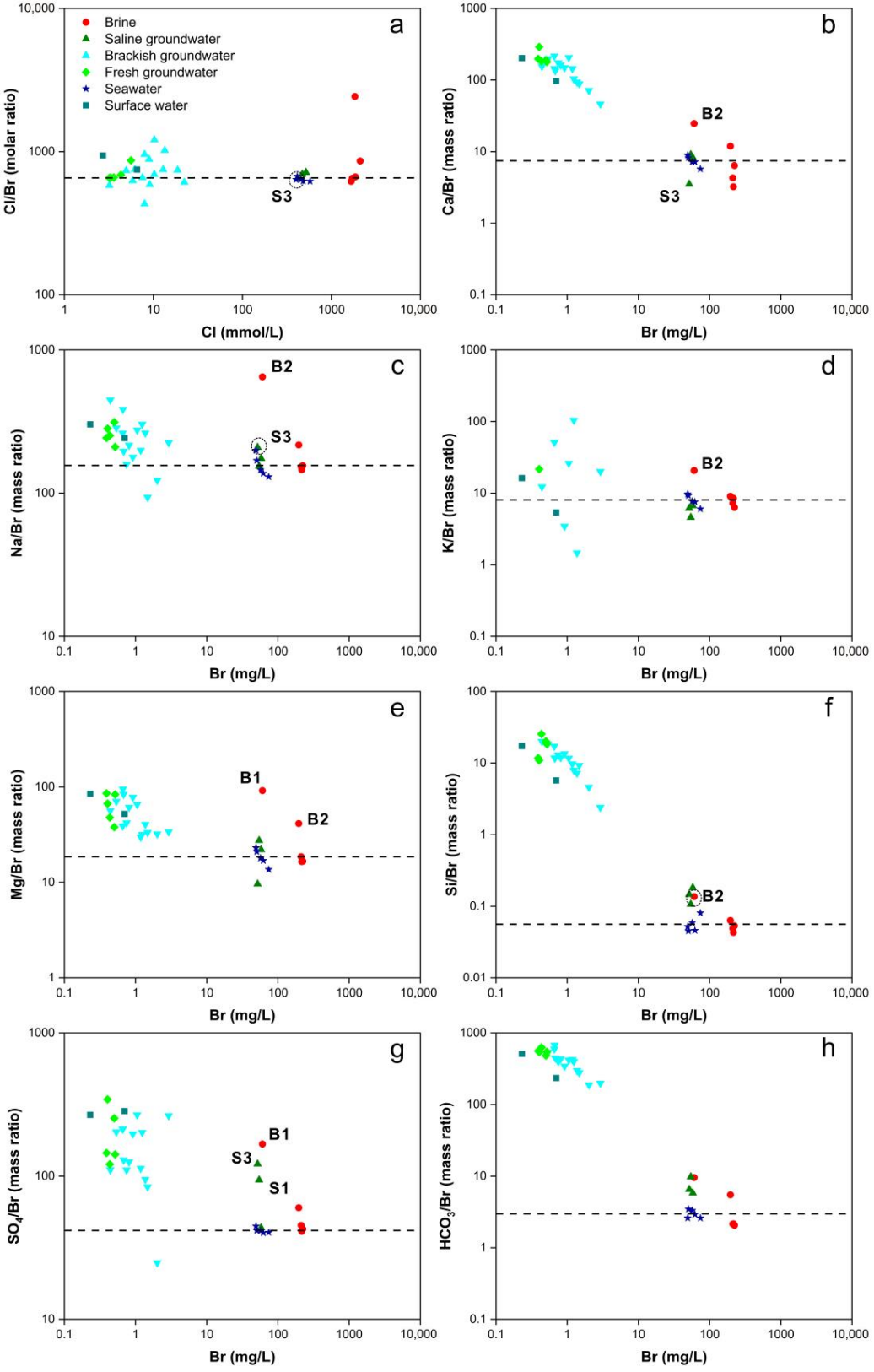

Figure 4. Diagrams of the relationship between Cl/Br and Cl^- and the relationships between Ca^{2+}, Na^+, K^+, Mg^{2+}, Si^{4+}, SO_4^{2-}, HCO_3^- normalized to Br^- and Br^- of all water samples. (**a**) Cl/Br and Cl^- (**b**) Ca^{2+} and Br^- (**c**) Na^+ and Br^- (**d**) K^+ and Br^- (**e**) Mg^{2+} and Br^- (**f**) Si^{4+} and Br^- (**g**) SO_4^{2-} and Br^- (**h**) HCO_3^- and Br^-.

The Ca/Br ratios for brine and saline groundwater closely resemble those of seawater (Figure 4b), indicating their marine origin. However, sample B2 exhibits significantly elevated Ca^{2+} concentrations, likely attributed to the dissolution of minerals such as limestone and calcite. In contrast, the lower Ca^{2+} concentration in sample S3 may be due to cation exchange adsorption processes. The Ca/Br ratios for brackish and fresh groundwater are considerably higher than those for seawater, approaching values observed in surface water (Figure 4b). This suggests that both brackish and fresh groundwater are primarily influenced by precipitation and the dissolution of carbonate minerals, with minimal impact from seawater. Han et al. (2011) [7] simulated the dissolution processes of calcite and gypsum, and the precipitation process of aragonite, confirming ion exchange between Ca^{2+}, Mg^{2+}, and Na^{+} (Equations (2) and (3)). They also confirmed the existence of mixing between fresh groundwater and saline groundwater. However, in this study, the majority of samples were distributed along the mixing line, and ion exchange was observed only in a minority of samples. This suggests that ion exchange is not a universally occurring process, consistent with the findings of Du et al. (2015) [44]. The study by Zhang et al. (2017) [86] posits that ion exchange processes only occur at the interface between the fresh groundwater and saline water in the mixture along hydraulic gradients.

$$Na(K) - Solid + Ca^{2+}\left(Mg^{2+}\right)aq = 2Na(K)aq + Ca(Mg) - Solid^{++} \quad (2)$$

$$2Na(K)aq - Ca(Mg) - Solid = 2Na(K) - Solid - Ca^{2+}\left(Mg^{2+}\right)aq \quad (3)$$

The Na/Br and K/Br ratios for brine and saline groundwater closely resemble those of seawater (Figure 3c,d), indicating their marine-derived salinity. However, sample B2 displays significantly higher Na^{+} and K^{+} concentrations, possibly attributed to the weathering of minerals such as mica, feldspar, or clay minerals. Elevated Na concentrations in sample S3 suggest the presence of cation exchange adsorption processes. Brackish and fresh groundwater exhibit more substantial fluctuations in Na/Br and K/Br ratios (Figure 3c,d), differing significantly from seawater and surface water. These variations may be linked to the dissolution of clay minerals and cation exchange adsorption processes.

The Mg/Br ratios for brine and saline groundwater closely resemble those of seawater (Figure 4e). However, samples B1 and B2 display considerably higher Mg^{2+} concentrations, indicative of the dissolution of silicate and sulfate minerals, or processes involving the precipitation of limestone and calcite. In contrast, brackish and fresh groundwater exhibit Mg/Br ratios resembling those of surface water.

Except for sample B2, the Si/Br ratios for brine closely resemble those of seawater (Figure 4f). However, both saline groundwater and sample B2 exhibit significantly higher Si^{4+} concentrations than seawater, suggesting processes involving the dissolution of silicate minerals. Brackish and fresh groundwater Si/Br ratios resemble those of surface water, indicating their primary influence from precipitation and silicate mineral dissolution.

The SO_4/Br ratios for most brine and saline groundwater samples closely resemble those of seawater (Figure 4g). Nevertheless, samples B2, S1, and S3 exhibit markedly higher $SO_4{}^{2+}$ concentrations than seawater, indicating the presence of sulfate mineral dissolution processes. This suggests that brine and saline groundwater may exist in reducing environments. Brackish and fresh groundwater exhibit more substantial fluctuations in SO_4/Br ratios (Figure 4g), potentially associated with industrial activities.

$HCO_3{}^{-}$ concentrations are related to the dissolution and precipitation of carbonate minerals. The $HCO_3{}^{-}$ concentrations for brine and saline groundwater closely resemble those of seawater but are higher than seawater (Figure 4h), signifying their marine origin. In contrast, brackish and fresh groundwater $HCO_3{}^{-}$ concentrations resemble those of surface water.

$NO_3{}^{-}$ concentrations in the northern plain area of the study region are relatively high, while concentrations in the southern mountainous areas and the southwestern plain region are lower (Figure 5). It is widely acknowledged that $NO_3{}^{-}$ concentrations are

closely associated with human activities, particularly agricultural practices and irrigation, which are likely the primary contributors to NO_3^- levels. The northern plain area encompasses a substantial expanse of cultivated land and experiences intensive fertilizer usage, which significantly elevates NO_3^- concentrations in this region. In contrast, the southern mountainous terrain and the southwestern plain area are characterized by rugged topography. In the latter, industrial and aquaculture activities predominate over extensive agriculture, leading to smaller areas of cultivated land and reduced fertilizer application rates. Consequently, these factors result in lower NO_3^- concentrations in these regions.

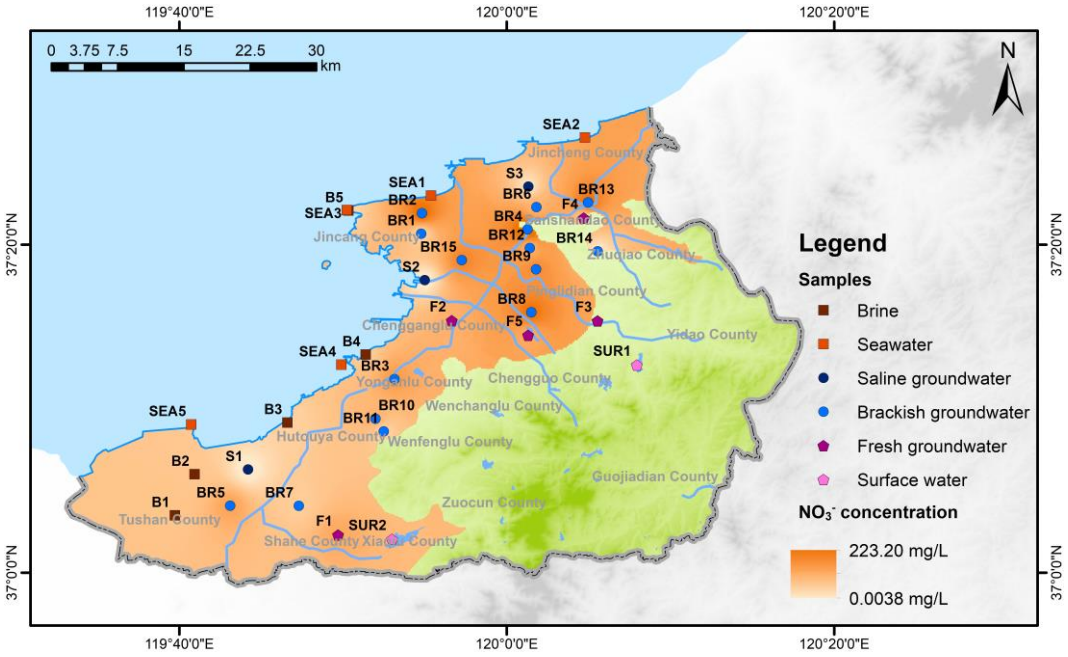

Figure 5. Diagram of NO_3^- concentration of all groundwater samples.

3.2. Hydrogen and Oxygen Isotope Compositions

The Global Meteoric Water Line (GMWL) and the Local Meteoric Water Line (LMWL), expressed as $\delta^2H = 8 \times \delta^{18}O + 10$ and $\delta^2H = 7.8 \times \delta^{18}O + 6.3$, respectively, are depicted in Figure 6 [87]. The δ^2H and $\delta^{18}O$ values for all samples fall within the range of −61.8‰ to −9.2‰ and −8.7‰ to −0.7‰, respectively. The majority of water samples are situated to the right of both precipitation lines, and exhibit a consistent alignment with an evaporation line, defined as $\delta^2H = 6.15 \times \delta^{18}O - 9.17$. The slope of the evaporation line is lower than that of the GMWL and LMWL, indicating lower precipitation and a more pronounced evaporation effect. Sample B14 stands out with the lowest hydrogen and oxygen isotope values, reflecting characteristics akin to ancient atmospheric precipitation or paleo-runoff. Conversely, seawater samples display the highest hydrogen and oxygen isotope values, indicative of pronounced evaporative processes.

Brackish and fresh groundwater samples closely adhere to the Local Meteoric Water Line (LMWL), signifying their primary source as atmospheric precipitation. In contrast, brine, seawater, saline groundwater samples, and a subset of brackish groundwater samples align with the evaporation line, emphasizing the pivotal role of evaporation processes in shaping groundwater salinity and H-O isotope compositions. This alignment also underscores the complex mixing dynamics within the groundwater systems. Notably, despite brine exhibiting higher total dissolved solids (TDS) compared to seawater, there is a conspicuous depletion pattern in the H-O isotopes. This phenomenon likely stems from a period during which brine experienced mixing with atmospheric precipitation or surface water, potentially occurring during a relatively cooler phase after the brine's formation. Surface water samples markedly deviate from the LMWL, clustering prominently along

the evaporation line, signifying a history of significant evaporation processes within the study area.

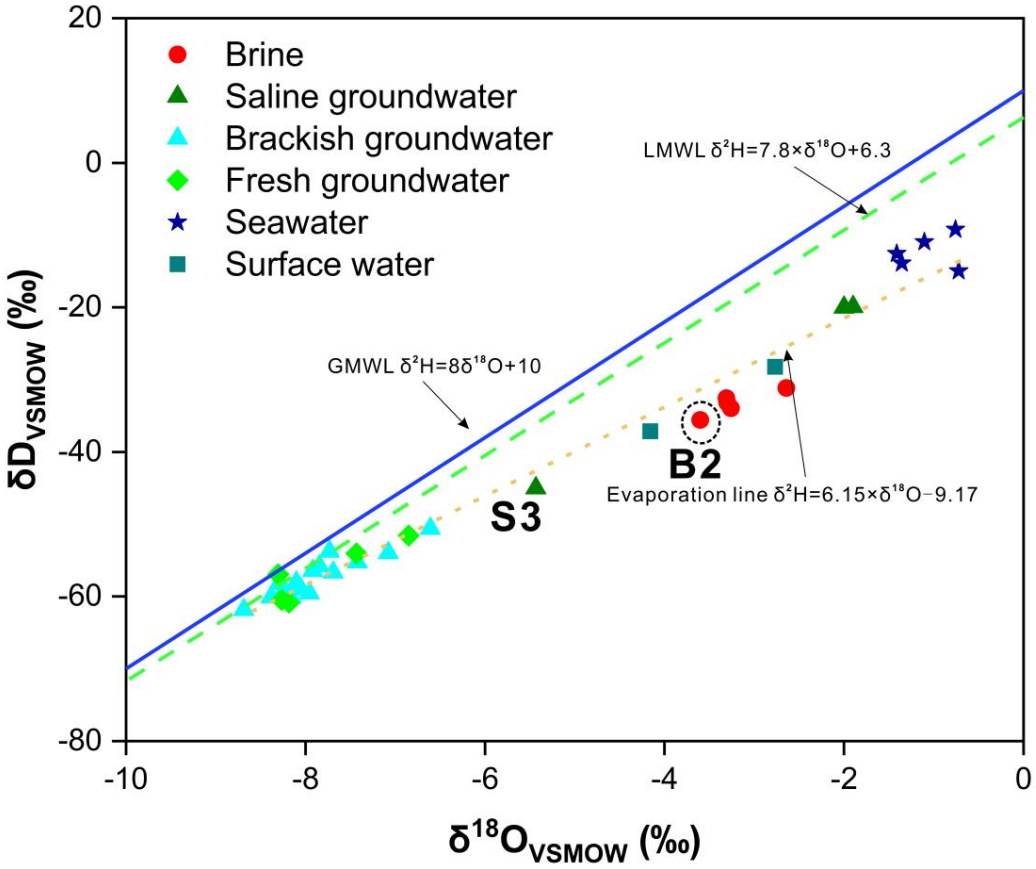

Figure 6. Diagrams of the relationship between δ^2H and $\delta^{18}O$ values of all water samples.

Samples S1 and S2 are positioned between seawater and brine, signifying their susceptibility to seawater intrusion within the brine aquifer. Conversely, sample S3 displays notably lower H-O isotope values than S1 and S2, approaching the values observed in brackish and fresh groundwater samples. This observation points to an alternative mixing process, characterized by distinct features associated with atmospheric precipitation.

Figure 7a illustrates the relationship between $\delta^{18}O$ values and Cl^- concentrations. If a mixture of freshwater and seawater is present in the groundwater, $\delta^{18}O$ values and Cl^- concentrations should exhibit a positive correlation [88]. The $\delta^{18}O$ of brackish groundwater registers lower values compared to seawater, while the Cl^- concentrations are notably higher, indicative of an evaporation–concentration process. Brackish groundwater and several saline groundwater areas fall within the mixing area between seawater and fresh groundwater. As Cl^- concentrations increase, $\delta^{18}O$ values gradually approach those of seawater, indicating a process of mixing between seawater and fresh groundwater. Brackish groundwater and fresh groundwater deviate from the mixing area, exhibiting Cl^- concentrations similar to surface water, and lower $\delta^{18}O$ values, indicating the influence of atmospheric precipitation and evaporation effects during the infiltration process.

The d-excess was calculated using Equation (4) to elucidate the atmospheric water vapor circulation process (Figure 7b). The negative d-excess in brine is related to the evaporation–concentration process it undergoes during formation. Surface water samples collected from the edges of two reservoirs have experienced prolonged evaporation, resulting in low d-excess values similar to seawater. Saline groundwater is considered a mixture of seawater and fresh groundwater, hence also exhibiting low d-excess values. The higher

d-excess values in brackish and fresh groundwater samples reflect their closer connection to precipitation and a higher proportion of recycled water vapor [88].

$$d - excess = \delta D - 8 \times \delta^{18}O \quad (4)$$

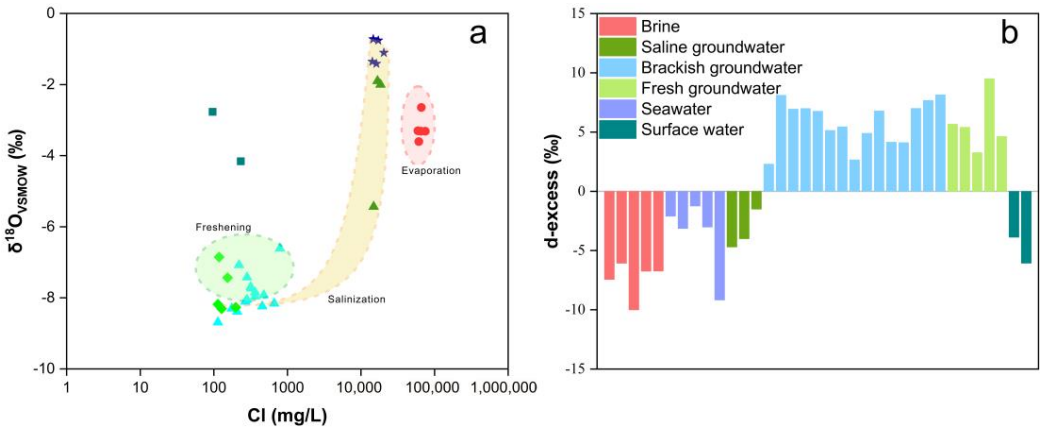

Figure 7. Diagrams of the relationship between $\delta^{18}O$ value and Cl^- and d-excess of all water samples. (**a**) Relationship between $\delta^{18}O$ value and Cl^- (**b**) d-excess.

3.3. Chlorine Isotope Compositions

The relationship between $\delta^{37}Cl$ and Cl^- concentrations for brine and seawater is illustrated in Figure 8. $\delta^{37}Cl$ values in brine samples range from −1.08‰ to −0.04‰, while seawater $\delta^{37}Cl$ values span from −0.70‰ to 0.22‰. Brine samples, especially those influenced by seawater evaporation, consistently demonstrate negative $\delta^{37}Cl$ values, indicating a distinct depletion pattern in $\delta^{37}Cl$.

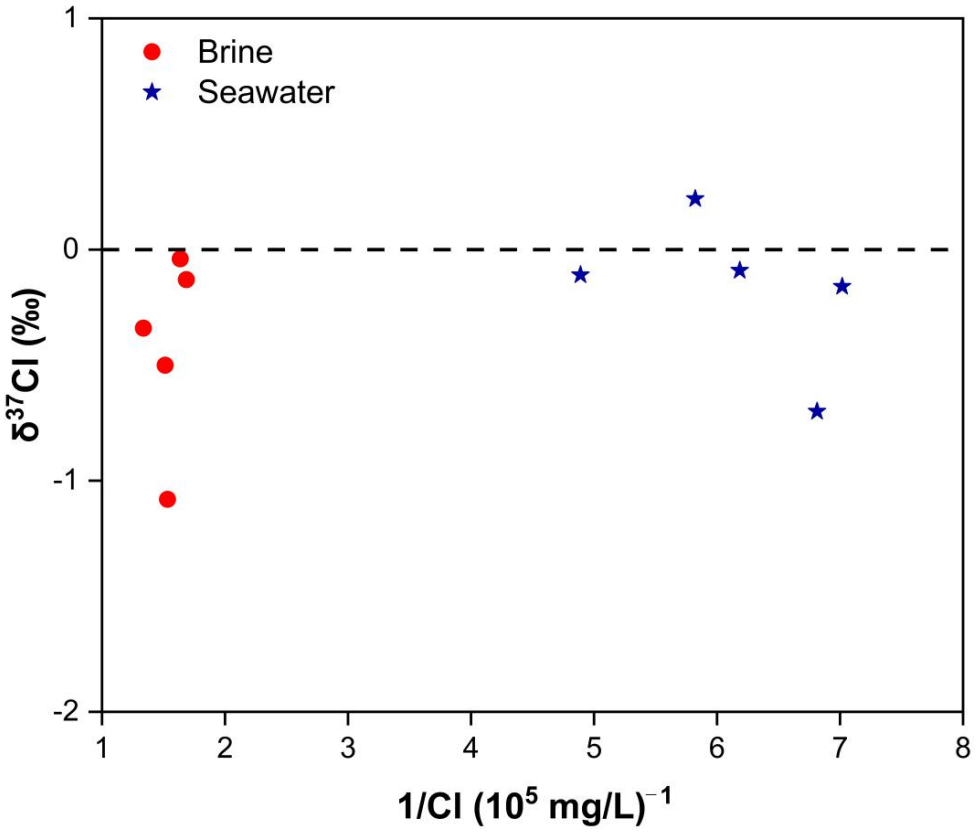

Figure 8. Diagram of $\delta^{37}Cl$ and 1/Cl values of brine samples and seawater samples.

During the process of seawater evaporation, gradual rock salt precipitation and concurrent recrystallization result in the enrichment of $\delta^{37}Cl$ in the solid phase, while the liquid phase exhibits a depletion pattern in $\delta^{37}Cl$ [89]. Consequently, brine originating from the dissolution of rock salt also displays negative $\delta^{37}Cl$ values. However, brine associated with rock salt dissolution typically exhibits Cl/Br ratios significantly higher than those found in seawater. Figure 4a reveals that the Cl/Br ratios in brine closely resemble those in seawater, suggesting that the primary source of brine is not primarily linked to the dissolution of rock salt. Conversely, brine sample B2 stands out with a Cl/Br ratio of 2426.81, significantly exceeding that of seawater, thus aligning with characteristics consistent with rock salt dissolution.

4. Discussion

4.1. Genesis of Brine: Seawater Evaporation, Halogen Precipitation, and Water–Rock Interaction

The formation of brine aquifers in the Bohai Sea region results from a complex interplay of climate change, tectonic movements, and multiple episodes of sea–land evolution [90]. The initial development of lagoons in this area occurred during the early stages of seawater regression [91]. As lagoons lacked natural drainage outlets, they experienced prolonged periods of evaporation. Over time, lagoon water infiltrated the deeper subsurface, ultimately converging at the forefront of ancient deltas [1].

During the process of evaporation and infiltration, various salts, including carbonates, sulfates, sodium salts, potassium salts, and magnesium salts, became concentrated and precipitated within the lagoon water, eventually forming sedimentary salts [92]. The study area has experienced three marine transgressions since the Late Pleistocene [7]. In subsequent marine transgressions, the mixing of sedimentary rocks with ancient seawater led to the dissolution of soluble salts back into the liquid phase, as shown in Figure 4, while insoluble carbonates and sulfates remained as part of the sedimentary salts [93].

As the sea regressed, a layer of continental sediments, primarily composed of clay and subclay, covered the brine, acting as a barrier to further infiltration of ancient atmospheric precipitation. At this stage, the brine entered a transitional phase, with water–rock interactions becoming predominant [92].

Figure 6 demonstrates the proximity of brine samples to the evaporation line, while Figure 8 showcases negative $\delta^{37}Cl$ values in the brine, signifying a substantial evaporation process during its formation. Typically, as the proportion of fresh groundwater increases, both Cl^- concentration and $\delta^{37}Cl$ decrease [94]. The negative $\delta^{37}Cl$ values observed in brine, when compared to seawater, provide clear evidence of brine's interaction with ancient atmospheric precipitation during its genesis [93]. Han et al. (2011) [7] suggest that this isotopic-depletion characteristic may also be attributed to mixing with depleted runoff from the continental margins.

4.2. Genesis of Saline Groundwater: Evaporation of Seawater and Mixing Processes

Figure 4 illustrates relatively minor fluctuations in cation concentrations for saline groundwater, which is slightly elevated compared to seawater except K^+. These findings highlight the impact of evaporated seawater on the formation of saline groundwater. Figure 6 positions saline groundwater to the right of the evaporation line, situated between brine and seawater. This positioning implies that the genesis of saline groundwater involves a combination of brine and seawater mixing, alongside a significant evaporation component. Notably, Sample S3 shows a closer affinity to brackish and fresh groundwater, suggesting the influence of atmospheric precipitation during its formation. Ma et al. (2007) [95] also confirmed two origins of saline groundwater: the mixing of brine with seawater and the mixing of brine with freshwater. Liu et al. (2017) [39] proposed that, within the mixing process between brine and seawater, saline groundwater received an additional fresh groundwater input, potentially originating from atmospheric precipitation and river water sources. Subsequently, the saline groundwater reservoir became enclosed, and no longer susceptible to the influence of other water sources.

4.3. Genesis of Brackish Groundwater: Atmospheric Precipitation and Human Activities

Figure 4 depicts the scattered distribution of Cl/Br ratios in brackish groundwater. The ratios of cations to Br^- in this type of groundwater tend to be generally higher compared to seawater and saline groundwater, bearing a closer resemblance to fresh groundwater. These observations suggest that the formation of brackish groundwater was not significantly influenced by seawater or saline groundwater. In Figure 6, brackish groundwater is positioned proximate to the LMWL, signifying that its formation is influenced by atmospheric precipitation. For the majority of brackish groundwater samples, there is a departure from the evaporation line, implying that the mixing of saline groundwater and fresh groundwater had a limited impact on their formation process. ^{14}C testing results also indicate a rapid exchange between brackish groundwater and atmospheric precipitation [7]. It is worth noting that the brackish groundwater samples in this study are all from Holocene groundwater. Liu et al. (2017) [39] suggested that brackish groundwater in the Late Pleistocene groundwater formed through a process of mixing between saline and fresh groundwater. On the other hand, Du et al. (2015) [44] discussed the characteristics of 81Br and suggested that another potential source of brackish groundwater could be marine aerosols.

In comparison to brine and saline groundwater, brackish groundwater exhibits notably higher NO_3^- concentrations, displaying a discernible and systematic concentration gradient. As depicted in Figure 5, the northern plain area exhibits elevated NO_3^- concentrations, while other regions show lower NO_3^- levels. The northern plain area is predominantly characterized by agricultural land use, where the application of pesticides and fertilizers containing substantial NO_3^- content is prevalent. Consequently, NO_3^- infiltrates into the brackish groundwater aquifer through agricultural irrigation practices. The variability in NO_3^- concentrations within the northern plain area can be attributed to differences in the intensity of fertilizer application. Conversely, the southeastern mountainous area has limited cultivated land, and the southwestern plain area is primarily allocated for industrial and aquaculture purposes, resulting in a reduced usage of pesticides and fertilizers and consequently lower NO_3^- concentrations. Therefore, human activities, particularly agricultural practices, are regarded as crucial contributors to the genesis of brackish groundwater.

4.4. Limitations and Future Research

In the sample testing process, only seawater and brine samples were tested for $\delta^{37}Cl$. This was due to limitations in the Cl^- concentrations of other samples and the constraints of existing testing equipment and methods. It does not imply that $\delta^{37}Cl$ in other samples is unimportant.

The acceptable range of IBE exhibits some variations in different studies. Hem (1985) [96] indicated that samples with a TDS less than 1 g/L typically have IBEs not exceeding 1–2%, while samples with a higher TDS can accommodate larger IBEs. Appelo and Postma (2005) [97] suggested that an IBE exceeding 5% should be considered anomalous. Li et al. (2016) [74] and Bouaissa et al. (2021) [98] considered test results with IBE more than 9% and 10% as accurate, respectively. In two other studies, test results with IBEs exceeding 10% were also deemed acceptable [19,99]. In this study, 53% of the samples exhibited IBEs within 5%, while the IBEs for all samples remained within 10% (Table S1). Fritz (1994) [100] suggested that these errors might be due to limitations in the testing equipment and measurement techniques, or carelessness in their operation. In this study, checks were implemented across all procedures to ensure accuracy, and each sample was subjected to three replicate experiments to confirm the reliability of the test results. Atkinson (2023) [101] suggested that the volatilization or dissociation of HCO_3^- during on-site testing was the reason for the underestimation of its concentration, leading to the positive IBE in some samples. In addition, significant IBE could potentially arise from a maximum testing error of 5% attributable to the testing technique, as well as the presence of untested ion species in the water samples.

The sampling for this study was conducted in September 2020, and the test results of the samples can only reflect the groundwater's hydrochemical composition and isotope characteristics during the sampling period. A study by Wang et al. (2019) [102] demonstrated that seawater intrusion and groundwater salinization are dynamic processes. Additionally, several studies have shown that the stable hydrogen and oxygen isotope content in various water bodies varies with different seasons and months [88,95]. Investigating the evolution of groundwater quality, especially the interannual and seasonal dynamics of groundwater salinization, is necessary for preventing and mitigating seawater intrusion and for the sustainable utilization of groundwater resources. This study recommends the establishment of long-term monitoring points at appropriate locations in the study area to achieve this goal.

5. Conclusions

This study employed hydrochemical and isotope analyses (H, O, Cl) to investigate the intricate mechanisms underpinning groundwater salinization within the Quaternary aquifers of the eastern coastal plain of Laizhou Bay. This study complements other studies in the area also unraveling the water dynamics in this important area. The findings underscore that the formation of brine and saline groundwater is driven by the process of seawater evaporation, whereas the genesis of brackish groundwater exhibits minimal associations with seawater. Furthermore, an examination through H-O isotope analyses substantiates the prominent role of evaporation in shaping the characteristics of brine. In contrast, saline groundwater originates from a complex mixing process involving brine, seawater, and freshwater. Conversely, brackish groundwater primarily derives its composition from atmospheric precipitation, distinctly reflecting the H-O isotope signatures associated with this source. Furthermore, a rigorous assessment utilizing stable chlorine isotope analysis elucidates that the principal source of brine can be attributed to the evaporation of seawater and the dissolution of rock salt.

The formation of brine is emblematic of a dynamic interplay between climatic fluctuations, tectonic dynamics, and episodes of sea regression and transgression. It is underscored by the progressive transformation of ancient seawater through a series of stages, including pronounced evaporation and the dissolution of rock salt, culminating in the creation of brine. Conversely, the emergence of saline groundwater is guided by the amalgamation of brine and seawater, transitioning subsequently into a self-contained environment marked by evaporation. The formation of brackish groundwater primarily arises from the influence of atmospheric precipitation, exhibiting limited correlations with seawater or saline groundwater. Additionally, human activities, particularly agricultural practices, exert a substantial impact on NO_3^- concentrations within brackish groundwater, with agricultural irrigation being the predominant contributory factor.

This study provides an example of the intricate mechanisms that govern groundwater salinization within the Quaternary aquifers of the eastern coastal plain of Laizhou Bay, encompassing multifaceted aspects such as climate variability and sea–land evolution. These findings can help to advance our understanding of the processes underpinning groundwater genesis and preserve invaluable groundwater resources.

Supplementary Materials: The following supporting information can be downloaded at: https://www.mdpi.com/article/10.3390/w15203629/s1, Table S1: Hydrochemistry and stable isotope compositions of all water samples in the study area.

Author Contributions: Conceptualization, P.H.; methodology, P.H.; software, P.H.; validation, P.H.; formal analysis, C.M.; investigation, P.H.; resources, C.M.; data curation, P.H.; writing—original draft preparation, P.H.; writing—review and editing, A.Z.; visualization, P.H.; supervision, C.M.; project administration, A.Z.; funding acquisition, C.M. All authors have read and agreed to the published version of the manuscript.

Funding: This research was funded by the National Natural Science Foundation of China, grant number 41572212.

Data Availability Statement: The data are available on request from the corresponding author due to privacy restrictions.

Acknowledgments: The authors wish to thank the State Key Laboratory of Biogeology and Environmental Geology, China University of Geosciences, and the Salt Lake Chemistry Analysis and Test Center, Qinghai Institute of Salt Lakes, Chinese Academy of Sciences for their support in isotope analyses. The authors are grateful to the editor and reviewers for their suggestions.

Conflicts of Interest: The authors declare no conflict of interest.

References

1. He, Z.K.; Ma, C.M.; Zhou, A.G.; Qi, H.H.; Liu, C.F.; Cai, H.S.; Zhu, H.C. Using hydrochemical and stable isotopic (δ2H, δ18O, δ11B, and δ37Cl) data to understand groundwater evolution in an unconsolidated aquifer system in the southern coastal area of Laizhou Bay, China. *Appl. Geochem.* **2018**, *90*, 129–141. [CrossRef]
2. Yolcubal, I.; Gunduz, O.C.A.; Kurtulus, N. Origin of salinization and pollution sources and geochemical processes in urban coastal aquifer (Kocaeli, NW Turkey). *Environ. Earth Sci.* **2019**, *78*, 181. [CrossRef]
3. Sallam, O. New approach in estimation of seawater intrusion footprint (SWIF) for irrigated crops using coastal groundwater. *Groundw. Sustain. Dev.* **2022**, *18*, 100772. [CrossRef]
4. Wen, X.H.; Lu, J.; Wu, J.; Lin, Y.C.; Luo, Y.M. Influence of coastal groundwater salinization on the distribution and risks of heavy metals. *Sci. Total Environ.* **2019**, *652*, 267–277. [CrossRef]
5. Basack, S.; Bhattacharya, A.K.; Maity, P. A coastal groundwater management model with Indian case study. *Proc. Inst. Civ. Eng. Water Manag.* **2014**, *167*, 126–140. [CrossRef]
6. Barlow, P.M.; Reichard, E.G. Saltwater intrusion in coastal regions of North America. *Hydrol. J.* **2010**, *18*, 247–260. [CrossRef]
7. Han, D.M.; Kohfahl, C.; Song, X.F.; Xiao, G.Q.; Yang, J.L. Geochemical and isotopic evidence for palaeo-seawater intrusion into the south coast aquifer of Laizhou Bay, China. *Appl. Geochem.* **2011**, *26*, 863–883. [CrossRef]
8. Re, V.; Zuppi, G.M. Influence of precipitation and deep saline groundwater on the hydrological systems of Mediterranean coastal plains: A general overview. *Hydrol. Sci. J.* **2011**, *56*, 966–980. [CrossRef]
9. Anders, R.; Mendez, G.O.; Futa, K.; Danskin, W.R. A Geochemical Approach to Determine Sources and Movement of Saline Groundwater in a Coastal Aquifer. *Groundwater* **2014**, *52*, 756–768. [CrossRef]
10. Landes, A.A.L.; Aquilina, L.; Davy, P.; Vergnaud-Ayraud, V.; Le Carlier, C. Timescales of regional circulation of saline fluids in continental crystalline rock aquifers (Armorican Massif, western France). *Hydrol. Earth Syst. Sci.* **2015**, *19*, 1413–1426. [CrossRef]
11. Liu, H.; Gao, L.; Ma, C.; Yuan, Y. Analysis of the Seawater Intrusion Process Based on Multiple Monitoring Methods: Study in the Southern Coastal Plain of Laizhou Bay, China. *Water* **2023**, *15*, 2013. [CrossRef]
12. Kloppmann, W.; Negrel, P.; Casanova, J.; Klinge, H.; Schelkes, K.; Guerrot, C. Halite dissolution derived brines in the vicinity of a Permian salt dome (N German Basin). Evidence from boron, strontium, oxygen, and hydrogen isotopes. *Geochim. Cosmochim. Acta* **2001**, *65*, 4087–4101. [CrossRef]
13. Xaza, A.; Mapoma, H.W.T.; Abiye, T.A.; Clarke, S.; Kanyerere, T. Investigating Seawater Intrusion in Republic of South Africa's Heuningnes, Cape Agulhas Using Hydrogeochemistry and Seawater Fraction Techniques. *Water* **2023**, *15*, 2141. [CrossRef]
14. Zeng, W.J. Analysis on Change Characteristics of Soluble Silica in Shallow Groundwater of Coastal Area Caused by Seawater Intrusion. *J. Coast. Res.* **2018**, *83*, 282–286. [CrossRef]
15. Cary, L.; Casanova, J.; Gaaloul, N.; Guerrot, C. Combining boron isotopes and carbamazepine to trace sewage in salinized groundwater: A case study in Cap Bon, Tunisia. *Appl. Geochem.* **2013**, *34*, 126–139. [CrossRef]
16. Xu, X.Y.; Xiong, G.Y.; Chen, G.Q.; Fu, T.F.; Yu, H.J.; Wu, J.C.; Liu, W.Q.; Su, Q.; Wang, Y.C.; Liu, S.F.; et al. Characteristics of coastal aquifer contamination by seawater intrusion and anthropogenic activities in the coastal areas of the Bohai Sea, eastern China. *J. Asian Earth Sci.* **2021**, *217*, 104830. [CrossRef]
17. Green, T.R.; Taniguchi, M.; Kooi, H.; Gurdak, J.J.; Allen, D.M.; Hiscock, K.M.; Treidel, H.; Aureli, A. Beneath the surface of global change: Impacts of climate change on groundwater. *J. Hydrol.* **2011**, *405*, 532–560. [CrossRef]
18. Sivakumar, B. Global climate change and its impacts on water resources planning and management: Assessment and challenges. *Stoch. Environ. Res. Risk Assess.* **2011**, *25*, 583–600. [CrossRef]
19. Cary, L.; Petelet-Giraud, E.; Bertrand, G.; Kloppmann, W.; Aquilina, L.; Martins, V.; Hirata, R.; Montenegro, S.; Pauwels, H.; Chatton, E.; et al. Origins and processes of groundwater salinization in the urban coastal aquifers of Recife (Pernambuco, Brazil): A multi-isotope approach. *Sci. Total Environ.* **2015**, *530*, 411–429. [CrossRef]
20. Sithara, S.; Pramada, S.K.; Thampi, S.G. Impact of projected climate change on seawater intrusion on a regional coastal aquifer. *J. Earth Syst. Sci.* **2020**, *129*, 218. [CrossRef]
21. Wu, J.C.; Meng, F.H.; Wang, X.W.; Wang, D. The development and control of the seawater intrusion in the eastern coastal of Laizhou Bay, China. *Environ. Geol.* **2008**, *54*, 1763–1770. [CrossRef]
22. Li, J.; Gong, X.L.; Liang, X.; Liu, Y.; Yang, J.L.; Meng, X.M.; Alhassan, A. Salinity evolution of aquitard porewater associated with transgression and regression in the coastal plain of Eastern China. *J. Hydrol.* **2021**, *603*, 127050. [CrossRef]
23. Zhang, Z.L.; Liu, E.F.; Zhang, Y.; Xin, L.J. Environmental evolution in the salt-water intrusion area south of Laizhou Bay since late Pleistocene. *J. Geogr. Sci.* **2008**, *18*, 37–45. [CrossRef]

24. Chen, S.M.; Liu, H.W.; Liu, F.T.; Miao, J.J.; Guo, X.; Zhang, Z.; Jiang, W.J. Using time series analysis to assess tidal effect on coastal groundwater level in Southern Laizhou Bay, China. *J. Groundw. Sci. Eng.* **2022**, *10*, 292–301. [CrossRef]
25. Wen, X.H.; Diao, M.N.; Wang, D.; Gao, M. Hydrochemical characteristics and salinization processes of groundwater in the shallow aquifer of Eastern Laizhou Bay, China. *Hydrol. Process.* **2012**, *26*, 2322–2332. [CrossRef]
26. Sun, Y.; Xu, S.; Wang, Q.; Hu, S.; Qin, G.; Yu, H. Response of a Coastal Groundwater System to Natural and Anthropogenic Factors: Case Study on East Coast of Laizhou Bay, China. *Int. J. Environ. Res. Public Health* **2020**, *17*, 5204. [CrossRef]
27. Chen, Q.; Wei, J.; Wang, H.; Shi, L.; Gao, Z.; Liu, S.; Ning, F.; Jia, C.; Ji, Y.; Dong, F.; et al. Discussion on the Fluorosis in Seawater-Intrusion Areas Along Coastal Zones in Laizhou Bay and Other Parts of China. *Int. J. Environ. Res.* **2019**, *13*, 435–442. [CrossRef]
28. Han, D.M.; Song, X.F.; Currell, M.J.; Yang, J.L.; Xiao, G.Q. Chemical and isotopic constraints on evolution of groundwater salinization in the coastal plain aquifer of Laizhou Bay, China. *J. Hydrol.* **2014**, *508*, 12–27. [CrossRef]
29. Chafouq, D.; El Mandour, A.; Elgettafi, M.; Himi, M.; Chouikri, I.; Casas, A. Hydrochemical and isotopic characterization of groundwater in the Ghis-Nekor plain (northern Morocco). *J. Afr. Earth Sci.* **2018**, *139*, 1–13. [CrossRef]
30. Alfaifi, H.; Kahal, A.; Albassam, A.; Ibrahim, E.; Abdelrahman, K.; Zaidi, F.; Alhumidan, S. Integrated geophysical and hydrochemical investigations for seawater intrusion: A case study in southwestern Saudi Arabia. *Arab. J. Geosci.* **2019**, *12*, 372. [CrossRef]
31. Gopinath, S.; Srinivasamoorthy, K.; Saravanan, K.; Prakash, R. Tracing groundwater salinization using geochemical and isotopic signature in Southeastern coastal Tamilnadu, India. *Chemosphere* **2019**, *236*, 124305. [CrossRef]
32. Ezzeldin, H.A. Delineation of Salinization and Recharge Sources Affecting Groundwater Quality Using Chemical and Isotopic Indices in the Northwest Coast, Egypt. *Sustainability* **2022**, *14*, 16923. [CrossRef]
33. Gimenez-Forcada, E. Dynamic of Sea Water Interface using Hydrochemical Facies Evolution Diagram. *Groundwater* **2010**, *48*, 212–216. [CrossRef]
34. Gimenez-Forcada, E. Space/time development of seawater intrusion: A study case in Vinaroz coastal plain (Eastern Spain) using HFE-Diagram, and spatial distribution of hydrochemical facies. *J. Hydrol.* **2014**, *517*, 617–627. [CrossRef]
35. Amiri, V.; Nakhaei, M.; Lak, R.; Kholghi, M. Assessment of seasonal groundwater quality and potential saltwater intrusion: A study case in Urmia coastal aquifer (NW Iran) using the groundwater quality index (GQI) and hydrochemical facies evolution diagram (HFE-D). *Stoch. Environ. Res. Risk Assess.* **2016**, *30*, 1473–1484. [CrossRef]
36. Najib, S.; Fadili, A.; Mehdi, K.; Riss, J.; Makan, A. Contribution of hydrochemical and geoelectrical approaches to investigate salinization process and seawater intrusion in the coastal aquifers of Chaouia, Morocco. *J. Contam. Hydrol.* **2017**, *198*, 24–36. [CrossRef] [PubMed]
37. Bagheri, R.; Nosrati, A.; Jafari, H.; Eggenkamp, H.G.M.; Mozafari, M. Overexploitation hazards and salinization risks in crucial declining aquifers, chemo-isotopic approaches. *J. Hazard. Mater.* **2019**, *369*, 150–163. [CrossRef]
38. Pan, G.F.; Li, X.Q.; Zhang, J.; Liu, Y.D.; Liang, H. Groundwater-flow-system characterization with hydrogeochemistry: A case in the lakes discharge area of the Ordos Plateau, China. *Hydrol. J.* **2019**, *27*, 669–683. [CrossRef]
39. Liu, S.; Tang, Z.H.; Gao, M.S.; Hou, G.H. Evolutionary process of saline-water intrusion in Holocene and Late Pleistocene groundwater in southern Laizhou Bay. *Sci. Total Environ.* **2017**, *607*, 586–599. [CrossRef]
40. Bhandary, H.; Sabarathinam, C.; Al-Khalid, A. Occurrence of hypersaline groundwater along the coastal aquifers of Kuwait. *Desalination* **2018**, *436*, 15–27. [CrossRef]
41. Han, D.M.; Currell, M.J. Delineating multiple salinization processes in a coastal plain aquifer, northern China: Hydrochemical and isotopic evidence. *Hydrol. Earth Syst. Sci.* **2018**, *22*, 3473–3491. [CrossRef]
42. Bahir, M.; Ouhamdouch, S.; Carreira, P.M. Geochemical and isotopic approach to decrypt the groundwater salinization origin of coastal aquifers from semi-arid areas (Essaouira basin, Western Morocco). *Environ. Earth Sci.* **2018**, *77*, 485. [CrossRef]
43. Louvat, D.; Michelot, J.L.; Aranyossy, J.F. Origin and residence time of salinity in the Aspo groundwater system. *Appl. Geochem.* **1999**, *14*, 917–925. [CrossRef]
44. Du, Y.; Ma, T.; Chen, L.Z.; Shan, H.M.; Xiao, C.; Lu, Y.; Liu, C.F.; Cai, H.S. Genesis of salinized groundwater in Quaternary aquifer system of coastal plain, Laizhou Bay, China: Geochemical evidences, especially from bromine stable isotope. *Appl. Geochem.* **2015**, *59*, 155–165. [CrossRef]
45. Zghibi, A.; Zouhri, L.; Tarhouni, J. Groundwater modelling and marine intrusion in the semi-arid systems (Cap-Bon, Tunisia). *Hydrol. Process.* **2011**, *25*, 1822–1836. [CrossRef]
46. Hassen, I.; Hamzaoui-Azaza, F.; Bouhlila, R. Application of multivariate statistical analysis and hydrochemical and isotopic investigations for evaluation of groundwater quality and its suitability for drinking and agriculture purposes: Case of Oum Ali-Thelepte aquifer, central Tunisia. *Environ. Monit. Assess.* **2016**, *188*, 135. [CrossRef]
47. Shi, X.Y.; Wang, Y.; Jiao, J.J.; Zhong, J.L.; Wen, H.G.; Dong, R. Assessing major factors affecting shallow groundwater geochemical evolution in a highly urbanized coastal area of Shenzhen City, China. *J. Geochem. Explor.* **2018**, *184*, 17–27. [CrossRef]
48. Naeem, M.F.A.; Yusoff, I.; Ng, T.F.; Maity, J.P.; Alias, Y.; May, R.; Alborsh, H. A study on the impact of anthropogenic and geogenic factors on groundwater salinization and seawater intrusion in Gaza coastal aquifer, C Palestine: An integrated multi-techniques approach. *J. Afr. Earth Sci.* **2019**, *156*, 75–93. [CrossRef]
49. Kim, J.H.; Kim, K.H.; Thao, N.T.; Batsaikhan, B.; Yun, S.T. Hydrochemical assessment of freshening saline groundwater using multiple end-members mixing modeling: A study of Red River delta aquifer, Vietnam. *J. Hydrol.* **2017**, *549*, 703–714. [CrossRef]

50. Abd-Elhamid, H.; Abdelaty, I.; Sherif, M. Evaluation of potential impact of Grand Ethiopian Renaissance Dam on Seawater Intrusion in the Nile Delta Aquifer. *Int. J. Environ. Sci. Technol.* **2019**, *16*, 2321–2332. [CrossRef]
51. Christelis, V.; Mantoglou, A. Pumping Optimization of Coastal Aquifers Using Seawater Intrusion Models of Variable-Fidelity and Evolutionary Algorithms. *Water Resour. Manag.* **2019**, *33*, 555–568. [CrossRef]
52. Meyer, R.; Engesgaard, P.; Sonnenborg, T.O. Origin and Dynamics of Saltwater Intrusion in a Regional Aquifer: Combining 3-D Saltwater Modeling With Geophysical and Geochemical Data. *Water Resour. Res.* **2019**, *55*, 1792–1813. [CrossRef]
53. Paldor, A.; Shalev, E.; Katz, O.; Aharonov, E. Dynamics of saltwater intrusion and submarine groundwater discharge in confined coastal aquifers: A case study in northern Israel. *Hydrol. J.* **2019**, *27*, 1611–1625. [CrossRef]
54. Yu, X.; Michael, H.A. Mechanisms, configuration typology, and vulnerability of pumping-induced seawater intrusion in heterogeneous aquifers. *Adv. Water Resour.* **2019**, *128*, 117–128. [CrossRef]
55. Coplen, T.B.; Bohlke, J.K.; De Bievre, P.; Ding, T.; Holden, N.E.; Hopple, J.A.; Krouse, H.R.; Lamberty, A.; Peiser, H.S.; Revesz, K.; et al. Isotope-abundance variations of selected elements—(IUPAC Technical Report). *Pure Appl. Chem.* **2002**, *74*, 1987–2017. [CrossRef]
56. Gonfiantini, R.; Wassenaar, L.I.; Araguas-Araguas, L.; Aggarwal, P.K. A unified Craig-Gordon isotope model of stable hydrogen and oxygen isotope fractionation during fresh or saltwater evaporation. *Geochim. Cosmochim. Acta* **2018**, *235*, 224–236. [CrossRef]
57. Eissa, M.A.; Shawky, H.; Samy, A.; Khalil, M.M.H.; El Malky, M. Geochemical and Isotopic Evidence of Groundwater Salinization Processes in El Dabaa Area, Northwestern Coast, Egypt. *Geosciences* **2018**, *8*, 392. [CrossRef]
58. Carreira, P.M.; Lobo de Pina, A.; da Mota Gomes, A.; Marques, J.M.; Monteiro Santos, F. Radiocarbon Dating and Stable Isotopes Content in the Assessment of Groundwater Recharge at Santiago Island, Republic of Cape Verde. *Water* **2022**, *14*, 2339. [CrossRef]
59. Guo, X.Y.; Feng, Q.; Si, J.H.; Wei, Y.P.; Bao, T.; Xi, H.Y.; Li, Z.X. Identifying the origin of groundwater for water resources sustainable management in an arid oasis, China. *Hydrol. Sci. J.* **2019**, *64*, 1253–1264. [CrossRef]
60. Mohanty, A.K.; Rao, V. Hydrogeochemical, seawater intrusion and oxygen isotope studies on a coastal region in the Puri District of Odisha, India. *Catena* **2019**, *172*, 558–571. [CrossRef]
61. Nogueira, G.; Stigter, T.Y.; Zhou, Y.; Mussa, F.; Juizo, D. Understanding groundwater salinization mechanisms to secure freshwater resources in the water-scarce city of Maputo, Mozambique. *Sci. Total Environ.* **2019**, *661*, 723–736. [CrossRef]
62. Zhang, Y.P.; Li, Q.H.; Luo, Y.X.; Yan, L.; Peng, K.; Liu, Z.M.; Wang, Y.X. Groundwater salinization in a subtropical region, Beihai, southern China: Insights from hydrochemistry and multiple isotopes (H, O, S, Sr). *Appl. Geochem.* **2022**, *141*, 105323. [CrossRef]
63. Sreedevi, P.D.; Sreekanth, P.D.; Reddy, D.V. Influence of hydrological and hydrogeological factors on inland groundwater salinity in a hard rock aquifer, south India. *J. Earth Syst. Sci.* **2021**, *130*, 215. [CrossRef]
64. Kleine, B.I.; Stefansson, A.; Halldorsson, S.A.; Barnes, J.D. Impact of fluid-rock interaction on water uptake of the Icelandic crust: Implications for the hydration of the oceanic crust and the subducted water flux. *Earth Planet Sci. Lett.* **2020**, *538*, 116210. [CrossRef]
65. Liu, M.L.; Guo, Q.H.; Shi, H.J.; Cao, Y.Y.; Shang, J.B.; Zhang, M.Z. Chlorine geochemistry of various geothermal waters in China: Implications for geothermal system geneses. *J. Hydrol.* **2023**, *616*, 128783. [CrossRef]
66. Li, Y.P.; Jiang, S.Y.; Yang, T. Br/Cl, I/Cl and chlorine isotopic compositions of pore water in shallow sediments: Implications for the fluid sources in the Dongsha area, northern South China Sea. *Acta Oceanol. Sinica* **2017**, *36*, 31–36. [CrossRef]
67. Bagheri, R.; Nadri, A.; Raeisi, E.; Kazemi, G.A.; Eggenkamp, H.G.M.; Montaseri, A. Origin of brine in the Kangan gasfield: Isotopic and hydrogeochemical approaches. *Environ. Earth Sci.* **2014**, *72*, 1055–1072. [CrossRef]
68. Barnes, J.D.; Paulick, H.; Sharp, Z.D.; Bach, W.; Beaudoin, G. Stable isotope (delta O-18, delta D, delta Cl-37) evidence for multiple fluid histories in mid-Atlantic abyssal peridotites (ODP Leg 209). *Lithos* **2009**, *110*, 83–94. [CrossRef]
69. Agrinier, P.; Destrigneville, C.; Giunta, T.; Bonifacie, M.; Bardoux, G.; Andre, J.; Lucazeau, F. Strong impact of ion filtration on the isotopic composition of chlorine in young clay-rich oceanic sediment pore fluids. *Geochim. Cosmochim. Acta* **2019**, *245*, 525–541. [CrossRef]
70. Beaudoin, G.M.; Barnes, J.D.; John, T.; Hoffmann, J.E.; Chatterjee, R.; Stockli, D.F. Global halogen flux of subducting oceanic crust. *Earth Planet. Sci. Lett.* **2022**, *594*, 117750. [CrossRef]
71. Musashi, M.; Oi, T.; Kreulen, R. Chlorine isotopic compositions of deep saline fluids in Ibusuki coastal geothermal region, Japan: Using B-Cl isotopes to interpret fluid sources. *Isotopes Environ. Health Stud.* **2015**, *51*, 285–299. [CrossRef]
72. Madorsky, S.L.; Straus, S. Concentration of isotopes of chlorine by the countercurrent electromigration method. *J. Res. Natl. Bur. Stand.* **1947**, *38*, 185–189. [CrossRef]
73. Kaufmann, R.; Long, A.; Bentley, H.; Davis, S. Natural Chlorine Isotope Variations. *Nature* **1984**, *309*, 338–340. [CrossRef]
74. Li, J.; Wang, Y.; Xie, X. Cl/Br ratios and chlorine isotope evidences for groundwater salinization and its impact on groundwater arsenic, fluoride and iodine enrichment in the Datong basin, China. *Sci. Total Environ.* **2016**, *544*, 158–167. [CrossRef]
75. Fetter, C.W. *Applied Hydrogeology*; Waveland Press Inc.: Long Grove, IL, USA, 2018.
76. Salas, J.D.; Govindaraju, R.S.; Anderson, M.; Arabi, M.; Francés, F.; Suarez, W.; Lavado-Casimiro, W.S.; Green, T.R. Introduction to Hydrology. In *Modern Water Resources Engineering*; Wang, L.K., Yang, C.T., Eds.; Humana Press: Totowa, NJ, USA, 2014; pp. 1–126. [CrossRef]
77. Liu, Y.; Gan, Y.; Yu, T.; Liu, C.; Zhou, A. Online Simultaneous Determination of δD and δ18O in Micro-liter Water Samples by Thermal Conversion/Elemental Analysis-Isotope Ratio Mass Spectrometry. *Rock Miner. Anal.* **2010**, *29*, 643–647.

78. Liu, Y.D.; Zhou, A.G.; Gan, Y.Q.; Liu, C.F.; Yu, T.T.; Li, X.Q. An online method to determine chlorine stable isotope composition by continuous flow isotope ratio mass spectrometry (CF-IRMS) coupled with a Gasbench II. *J. Cent. South Univ.* **2013**, *20*, 193–198. [CrossRef]
79. Zhou, X.; Liu, S.; Miao, Q.; Han, B.; Wang, Z.; Hou, X.; Song, Z. The Hydro-chemical Feature and Prospect on Utilisation of Shallow Groundwater in Hengshui. In Proceedings of the International Conference on Energy and Environment Technology (ICEET 2009), Guilin, China, 16–18 October 2009; p. 859.
80. Gibbs, R.J. Mechanisms controlling world water chemistry. *Science* **1970**, *17*, 1088–1090. [CrossRef]
81. Alcala, F.J.; Custodio, E. Using the Cl/Br ratio as a tracer to identify the origin of salinity in aquifers in Spain and Portugal. *J. Hydrol.* **2008**, *359*, 189–207. [CrossRef]
82. Senthilkumar, M.; Gnanasundar, D. Application of Cl/Br ratio to demarcate the fresh-saline water interface in coastal aquifers of northern Tamilnadu, Southern India. *Groundw. Sustain. Dev.* **2021**, *15*, 100658. [CrossRef]
83. Selvakumar, S.; Chandrasekar, N.; Srinivas, Y.; Selvam, S.; Kaliraj, S.; Magesh, N.S.; Venkatramanan, S. Hydrogeochemical processes controlling the groundwater salinity in the coastal aquifers of Southern Tamil Nadu, India. *Mar. Pollut. Bull.* **2022**, *174*, 113264. [CrossRef] [PubMed]
84. Shin, K.; Koh, D.-C.; Jung, H.; Lee, J. The Hydrogeochemical Characteristics of Groundwater Subjected to Seawater Intrusion in the Archipelago, Korea. *Water* **2020**, *12*, 1542. [CrossRef]
85. Rajmohan, N.; Masoud, M.H.Z.; Niyazi, B.A.M. Impact of evaporation on groundwater salinity in the arid coastal aquifer, Western Saudi Arabia. *Catena* **2021**, *196*, 104864. [CrossRef]
86. Zhang, X.Y.; Miao, J.J.; Hu, B.X.; Liu, H.W.; Zhang, H.X.; Ma, Z. Hydrogeochemical characterization and groundwater quality assessment in intruded coastal brine aquifers (Laizhou Bay, China). *Environ. Sci. Pollut. Res.* **2017**, *24*, 21073–21090. [CrossRef]
87. Warr, O.; Giunta, T.; Onstott, T.C.; Kieft, T.L.; Harris, R.L.; Nisson, D.M.; Lollar, B.S. The role of low-temperature O-18 exchange in the isotopic evolution of deep subsurface fluids. *Chem. Geol.* **2021**, *561*, 120027. [CrossRef]
88. Jiao, R. *Spatial and Temporal Variations in Deuterium Excess of Tap Water across China and Their Significance for Water Source*; Northwest Normal University: Lanzhou, China, 2020. (In Chinese)
89. Liu, X.; Wei, H.Z.; Williams-Jones, A.; Ma, J.; Lu, J.J.; Jiang, S.Y.; Li, Y.C.; Dong, G. Chlorine isotope fractionation during serpentinization and hydrothermal mineralization: A density functional theory study. *Chem. Geol.* **2021**, *581*, 120406. [CrossRef]
90. Zheng, Y.; Gao, M.; Liu, S.; Wang, S.; Zhao, J.; Wang, C. Distribution characteristics of subsurface brine resources on the southern coast of laizhou bay since late pleistocene. *Hydrol. Eng. Geol.* **2014**, *41*, 11–18.
91. Zhang, S.Q.; Dai, F.C. Isotope and hydrochemical study of seawater intrusion in Laizhou Bay, Shandong Province. *Sci. China Ser. E-Tech. Sci.* **2001**, *44*, 86–91. [CrossRef]
92. Zhang, C.Y. *The Formation and Evolution of Underground Brine in the Coastal Plain of Laizhou Bay*; Chinese Academy of Geological Sciences: Beijing, China, 1993.
93. Qi, H.H.; Ma, C.M.; He, Z.K.; Hu, X.J.; Gao, L. Lithium and its isotopes as tracers of groundwater salinization: A study in the southern coastal plain of Laizhou Bay, China. *Sci. Total Environ.* **2019**, *650*, 878–890. [CrossRef] [PubMed]
94. Moussaoui, I.; Rosa, E.; Cloutier, V.; Neculita, C.M.; Dassi, L. Chemical and isotopic evaluation of groundwater salinization processes in the Djebeniana coastal aquifer, Tunisia. *Appl. Geochem.* **2023**, *149*, 105555. [CrossRef]
95. Ma, F.; Yang, Y.S.; Yuan, R.; Cai, Z.; Pan, S. Study of shallow groundwater quality evolution under saline intrusion with environmental isotopes and geochemistry. *Environ. Geol.* **2007**, *51*, 1009–1017. [CrossRef]
96. Hem, J.D. *Study and Interpretation of the Chemical Characteristics of Natural Water*; U. S. Geological Sruvey: Reston, VA, USA, 1985.
97. Appelo, C.A.; Postma, D. *Geochemistry, Groundwater and Pollution*, 2nd ed.; CRC Press: London, UK, 2005. [CrossRef]
98. Bouaissa, M.; Gharibi, E.; Ghalit, M.; Taupin, J.D.; El Khattabi, J. Identifying the origin of groundwater salinization in the Bokoya massif (central Rif, northern Morocco) using hydrogeochemical and isotopic tools. *Groundw. Sustain. Dev.* **2021**, *14*, 100646. [CrossRef]
99. Cruz, J.V.; Coutinho, R.; Pacheco, D.; Cymbron, R.; Antunes, P.; Freire, P.; Mendes, S. Groundwater salinization in the Azores archipelago (Portugal). *Environ. Earth Sci.* **2011**, *62*, 1273–1285. [CrossRef]
100. Fritz, S.J. A SURVEY OF CHARGE-BALANCE ERRORS ON PUBLISHED ANALYSES OF POTABLE GROUND AND SURFACE WATERS. *Groundwater* **1994**, *32*, 539–546. [CrossRef]
101. Atkinson, J.C. Assessment of major ions in groundwater supplied to Monterrey metropolitan area, Mexico: Quality assurance, technical analysis, and addenda. *Int. J. Environ. Sci. Technol.* **2023**. [CrossRef]
102. Wang, M.; Han, M.; Hui, H.K.; Li, Y.L. Study on seawater intrusion in Laizhou bay coastal zone based on groundwater model. *Int. J. Low-Carbon Technol.* **2019**, *14*, 222–226. [CrossRef]